



Cite this: *J. Mater. Chem. C*, 2017,
5, 5176

Synthesis of $\text{Mn}^{2+}:\text{Zn}_2\text{SiO}_4\text{-Eu}^{3+}:\text{Gd}_2\text{O}_3$ nanocomposites for highly sensitive optical thermometry through the synergistic luminescence from lanthanide-transition metal ions†

Feng Huang *^{abc} and Daqin Chen *^d

In this work, $\text{Mn}^{2+}:\text{Zn}_2\text{SiO}_4\text{-Eu}^{3+}:\text{Gd}_2\text{O}_3$ nanocomposites were fabricated following a multi-step solution route. The fluorescence intensity ratio of Mn^{2+} to Eu^{3+} in these composites exhibits remarkable temperature dependence, owing to the diverse thermal quenching behaviors of Mn^{2+} and Eu^{3+} ions. Using these nanomaterials to perform thermometry, excellent temperature sensitivity is achieved in the room temperature range. Specifically, the values of relative temperature sensitivity are all beyond $2.5\% \text{ K}^{-1}$ in the whole range of 303–323 K (*i.e.* 30–50 °C), and reach as high as $3.05\% \text{ K}^{-1}$ at 303 K, remarkably higher than those of other inorganic optical thermometric materials at a similar temperature. And the absolute sensitivities are all beyond 0.0089 K^{-1} in this temperature range, which is also a relatively high value. These results indicate the $\text{Mn}^{2+}:\text{Zn}_2\text{SiO}_4\text{-Eu}^{3+}:\text{Gd}_2\text{O}_3$ nanocomposites to be very promising nano-thermometric materials.

Received 7th April 2017,
Accepted 2nd May 2017

DOI: 10.1039/c7tc01500c

rsc.li/materials-c

1. Introduction

Fluorescence intensity ratio (FIR) based temperature sensing technology has recently attracted broad interest, due to its unique merits of non-contact, rapid response, as well as high spatial and temperature resolutions, which are in favor of thermometry in harsh environments, micro-systems or fast moving objects.^{1–8} In this technique, the FIR temperature probe (*i.e.* phosphors with temperature-dependent luminescence properties) is the critical part that determines the performance of a temperature sensing device. For an ideal FIR thermometric material, both high absolute and relative temperature sensitivities (S_a and S_r) are required, in the desired temperature detecting range.^{9–12}

Currently, urgent demands for temperature probing or mapping at a cellular level, microelectronic systems or nanomedicines, have

brought more stringent requirements for the thermometric material. To fulfill these applications, the candidate phosphors should possess sub-micro grain size,^{13,14} as well as both high absolute and relative temperature sensitivities in the room temperature range (typically, $S_a \geq 0.008 \text{ K}^{-1}$ and $S_r \geq 2\% \text{ K}^{-1}$ at 303–323 K).^{13,14}

The most conventional FIR materials are the lanthanide doped phosphors, in which the emission from thermally coupled level pairs (TCL) of the lanthanide ions (for example, $^2\text{H}_{11/2}$ and $^4\text{S}_{3/2}$ levels for Er^{3+}) is utilized as the temperature label.^{15–17} However, for these kinds of thermometric materials, the S_a values always reach their maximum at a temperature higher than 450 K (177 °C),¹¹ while at room temperature, few of them could be higher than 0.008 K^{-1} . More seriously, S_r of these FIR materials is highly related to the energy space (ΔE) between TCL pairs (typically, $S_r = \Delta E/kT^2$).⁹ For the most used TCL pairs, *i.e.* $^2\text{H}_{11/2}$ and $^4\text{S}_{3/2}$ levels for Er^{3+} ions, the S_r is only about $1.1\% \text{ K}^{-1}$ at 303 K (30 °C). Although the value of S_r can be increased by using the other TCL pairs with large ΔE , such as $^4\text{G}_{11/2}$ and $^2\text{H}_{9/2}$ levels of Er^{3+} ions, which can increase the S_r to about $2.2\% \text{ K}^{-1}$ (at 303 K),¹⁸ but concomitantly the S_a would be reduced to a very low value, owing to the weakening of thermal coupling between the TCL pair.

To achieve higher S_a and S_r , other thermometric strategies have been tried. For example the phonon assisted energy transfer between pairs of lanthanide ions (such as, the $\text{Tb}^{3+}/\text{Eu}^{3+}$ pair, the $\text{Nd}^{3+}/\text{Yb}^{3+}$ pair, as well as the $\text{Eu}^{3+}/\text{Nd}^{3+}$ pair). Qiu's group

^a College of Physics and Energy, Fujian Normal University, Fuzhou, Fujian, 350117, P. R. China. E-mail: fengh@fjnu.edu.cn

^b Fujian Provincial Key Laboratory of Quantum Manipulation and New Energy Materials, Fuzhou 350117, P. R. China

^c Fujian Provincial Collaborative Innovation Center for Optoelectronic Semiconductors and Efficient Devices, Xiamen 361005, P. R. China

^d College of Materials & Environmental Engineering, Hangzhou Dianzi University, Hangzhou, 310018, China. E-mail: dqchen@hdu.edu.cn

† Electronic supplementary information (ESI) available: Detailed deduction for eqn (3). See DOI: 10.1039/c7tc01500c

designed a doped NaGdF₄ core-shell nanostructure, and utilized the phonon assisted energy transfer from Tb³⁺ to Eu³⁺ to obtain a constant S_a of 0.012 K⁻¹ in a temperature range of 125–300 K, however the highest S_r in this temperature range was still not very high (only 0.5% K⁻¹).⁶ Qian's group constructed a Nd_{0.577}Yb_{0.423}BDC-F₄ metal-organic framework, to achieve the phonon assisted energy transfer from Nd³⁺ and Yb³⁺, which exhibits a maximum S_r of 0.816% K⁻¹ at 313 K.¹⁹ Yin's group used the energy transfer between Eu³⁺ and Nd³⁺ to achieve a maximum S_r of 2.58% K⁻¹ at 380 K; while at 303 K, the S_r was about 1.65% K⁻¹.²⁰

Intervalence charge transfer (IVCT) states inferred that lanthanide luminescence was another proposed strategy for developing thermometric materials with high temperature sensitivity. For example, Cao' group fabricated the Pr:KNa(NbO₃)₂ phosphor to achieve ultra-high S_r (8.7% K⁻¹ at 303 K), but concomitantly the S_a dropped down to a very low value at 303 K (according to the parameters from Cao's paper, the S_a can be estimated to be less than 0.0002 K⁻¹ at 303 K).²¹ In our previous works, we also made use of the IVCT participant's lanthanide luminescence, to construct several thermometric materials, such as Tb/Pr:NaGd(MoO₄)₂²² and Pr:Na₂La₂Ti₃O₁₀ micro-crystals.²³ For the former, the maximum S_a and S_r reach 0.097 K⁻¹ (at 483 K) and 2.05% K⁻¹ (at 403 K), respectively; while for the later the maximum S_a and S_r reach 0.40 K⁻¹ (at 543 K) and 1.96% K⁻¹ (at 443 K), respectively.

Obviously, the above-mentioned previous works have made great progress in promoting the maximum value of S_a or S_r , but simultaneously realizing both high S_a and S_r in the room temperature range (303–323 K) is still a great challenge. In addition, most of the thermometric materials developed so far still exhibit large grain sizes. Developing a highly sensitive thermometric material with sub-micro grain size is also a big challenge.

Herein, to achieve higher S_a and S_r at room temperature within a nano-sized thermometric material, we constructed Mn²⁺:Zn₂SiO₄-Eu³⁺:Gd₂O₃ nanocomposites. The strategy used in this study is the synergistic luminescence from Mn²⁺ and Eu³⁺ ions. As is well known, electron-phonon interaction in Mn²⁺:Zn₂SiO₄ belongs to the so called "strong coupling" system (the Huang-Rhys factor $S \gg 1$),^{24,25} in which the luminescence always presents a serious thermal quenching phenomenon. While electron-phonon interaction in Eu³⁺:Gd₂O₃ belongs to the "weak coupling" system (the Huang-Rhys factor $S \ll 1$),^{26,27} in which the luminescence is relatively insensitive against change in the temperature. Therefore, by integrating these two systems within a single nanostructure, it is possible to achieve a FIR with high temperature dependence. In this work, specifically, we synthesized the Mn²⁺:Zn₂SiO₄ nanorods with a diameter ranging from 50 to 100 nm, and then coated Eu³⁺:Gd₂O₃ nanoparticles on the surface of these nanorods, forming Mn²⁺:Zn₂SiO₄-Eu³⁺:Gd₂O₃ nanocomposites. As expected, the FIR of Eu³⁺ to Mn²⁺ in this nanomaterial exhibits remarkable temperature dependence. It is exciting that S_a and S_r of this material are calculated to be 0.0089 K⁻¹ and 3.05% K⁻¹, respectively, at room temperature (303 K), which are superior to those of the other inorganic

thermometric phosphors at the same temperature. Therefore, the Mn²⁺:Zn₂SiO₄-Eu³⁺:Gd₂O₃ nanocomposites can be regarded as very promising nano-thermometric materials. In addition, the strategy proposed in the present work, which integrates "weak/strong coupling" luminescence systems within a nano-composite for high performance thermometry, can also provide inspiration for developing novel optical temperature sensing materials.

2. Experimental

2.1. Chemical reagents

The used zinc nitrate hexahydrate (Zn(NO₃)₂·6H₂O), manganese chloride tetrahydrate (MnCl₂·4H₂O), tetraethyl orthosilicate (TEOS), polyethylene glycol (PEG, $M_N = 400$), gadolinium nitrate hexahydrate (Gd(NO₃)₃·6H₂O), europium nitrate hexahydrate (Eu(NO₃)₃·6H₂O), urea (CO(NH₂)₂), sodium hydroxide (NaOH) and ammonium hydroxide (NH₃, 35%) were purchased from Sinopharm Chemical Reagent Company.

2.2. Synthesis of the Mn²⁺:Zn₂SiO₄ nanorods

A hydrothermal reaction was carried out to synthesize Zn₂SiO₄ nanorods. In a typical synthesis, 10 mmol Zn(NO₃)₂·6H₂O, 1 ml TEOS, 2 g PEG and 1 ml 35% ammonium hydroxide were mixed in 40 ml deionized water. Then, 1 ml NaOH aqueous solution containing 0.8 g NaOH was dropped into the reaction solution. After being stirred for 15 min, this solution was transferred to a 50 ml Teflon-lined stainless autoclave. The autoclave was sealed and maintained at 200 °C for 48 h, and then cooled to room-temperature. A white precipitate was separated by centrifugation, washed with deionized water several times, and then dried at 80 °C for 6 h.

The doping of Mn²⁺ ions was achieved by including 1 mmol MnCl₂·4H₂O in the reaction solution.

2.3. Synthesis of the Mn²⁺:Zn₂SiO₄-Eu³⁺:Gd₂O₃ nanocomposites

In a typical synthesis, 1 g of the per-fabricated Mn²⁺:Zn₂SiO₄ nanorods was dispersed in 30 ml deionized water, followed by 0.97 mmol Gd(NO₃)₃·6H₂O, 0.03 mmol Eu(NO₃)₃·6H₂O, and 3 g urea and 2 g PEG. This mixture was kept in a 90 °C water bath for 4 h under stirring. After that, the products were filtered, washed with deionized water, and then calcined at 500 °C for 2 h.

2.4. Characterization

XRD analyses were carried out using a powder diffractometer (DMAX 2500) using Cu K_α radiation ($\lambda = 0.154$ nm). The morphology observation was conducted on a field emission SEM (JSM-6700F) working at 5 kV. Transmission electron microscopy (TEM), high resolution TEM (HRTEM) and selective area electron diffraction (SAED) were performed using a TEM (JEM-2010). PL spectra were measured using a spectrofluorometer (FLS 920) equipped with a xenon lamp (450 W). A temperature controlling stage (THMS 600) was used as the sample holder for

the temperature-dependent luminescence measurement. The actual chemical compositions of the sample were determined by the inductively coupled plasma (ICP) technique using a Perkin Elmer Optima 3300DV spectrometer.

3. Results and discussion

3.1. Synthesis process and structure of the $\text{Mn}^{2+}:\text{Zn}_2\text{SiO}_4-\text{Eu}^{3+}:\text{Gd}_2\text{O}_3$ nanocomposites

As schematically illustrated in Fig. 1, to fabricate the $\text{Mn}^{2+}:\text{Zn}_2\text{SiO}_4-\text{Eu}^{3+}:\text{Gd}_2\text{O}_3$ nanocomposites, firstly, we use a hydrothermal reaction to synthesize $\text{Mn}^{2+}:\text{Zn}_2\text{SiO}_4$ nanorods. The results of structural characterization for the first-step product are presented in Fig. 2 and 3. As demonstrated by XRD shown in Fig. 2, the product is identified to be hexagonal structured Zn_2SiO_4 (PDF 79-2005). No signal of impurities can be detected. Further SEM and TEM observations (Fig. 3) revealed that the products exhibit a rod-like shape with a diameter of 50–100 nm. HRTEM observation and the corresponding fast Fourier transform (FFT) pattern indicate that each nanorod is a single crystal, whose long axis is along the [001] direction, while the side exposures are identified to be {300} lattice planes, as displayed in Fig. 3c and d. The actual molar ratio of Mn^{2+} to Zn^{2+} in the $\text{Mn}^{2+}:\text{Zn}_2\text{SiO}_4$ product is

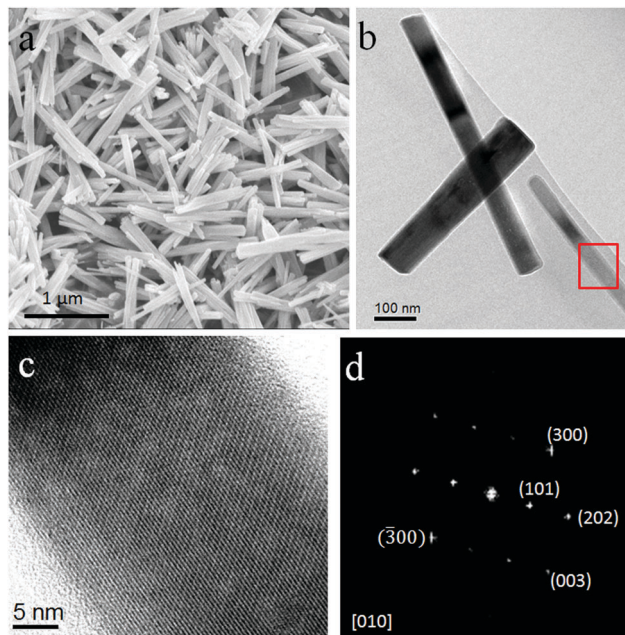


Fig. 3 (a) SEM and (b) TEM images of the $\text{Mn}^{2+}:\text{Zn}_2\text{SiO}_4$ products; (c) HRTEM and (d) corresponding fast Fourier transform (FFT) pattern for an individual $\text{Mn}^{2+}:\text{Zn}_2\text{SiO}_4$ nanorod.

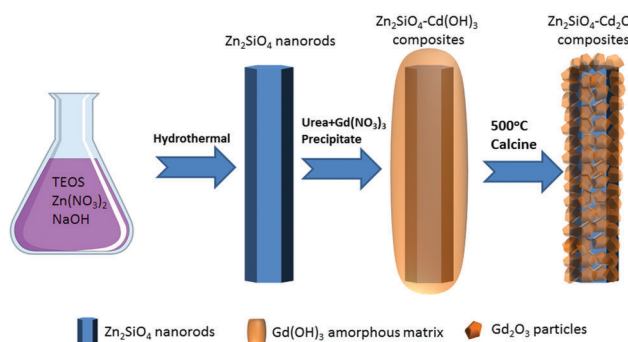


Fig. 1 Schematic illustration for the fabrication process of $\text{Mn}^{2+}:\text{Zn}_2\text{SiO}_4-\text{Eu}^{3+}:\text{Gd}_2\text{O}_3$ nanocomposites.

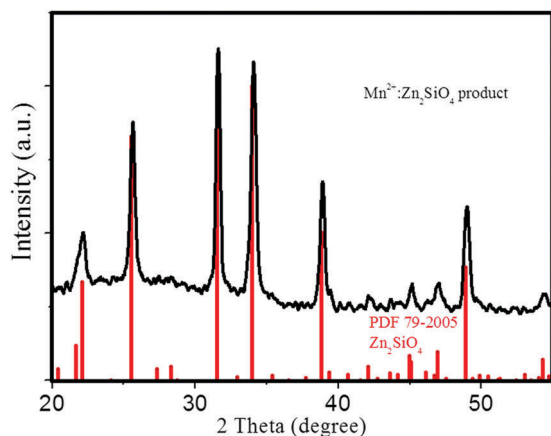


Fig. 2 XRD pattern of the $\text{Mn}^{2+}:\text{Zn}_2\text{SiO}_4$ products; bars on the bottom are the standard data of hexagonal Zn_2SiO_4 (PDF 79-2005).

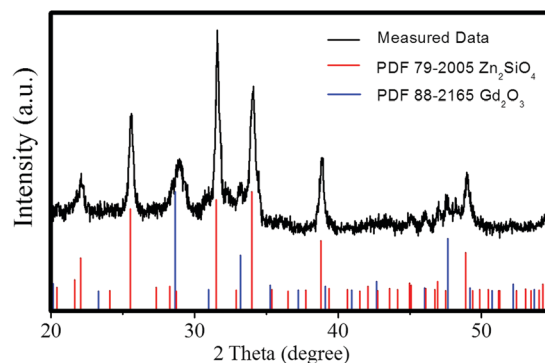


Fig. 4 XRD pattern of the $\text{Mn}^{2+}:\text{Zn}_2\text{SiO}_4-\text{Eu}^{3+}:\text{Gd}_2\text{O}_3$ composite product; bars on the bottom are standard data of the hexagonal Zn_2SiO_4 (red bars, PDF 79-2005) and cubic Gd_2O_3 (blue bars, PDF 8802165).

determined to be 5.78:94.22 by inductively coupled plasma (ICP) analysis.

The second step for fabricating $\text{Mn}^{2+}:\text{Zn}_2\text{SiO}_4-\text{Eu}^{3+}:\text{Gd}_2\text{O}_3$ nanocomposites is a urea assisted precipitation reaction for coating amorphous $\text{Eu}:\text{Gd}(\text{OH})_3$ on the surface of the $\text{Mn}^{2+}:\text{Zn}_2\text{SiO}_4$ nanorods, followed by calcination treatment for transforming the surficial $\text{Gd}(\text{OH})_3$ to Gd_2O_3 particles, as illustrated in Fig. 1. The results of structural characterization for the final products are presented in Fig. 4 and 5. As demonstrated by XRD shown in Fig. 4, the products are composed of hexagonal structured Zn_2SiO_4 and cubic structured Gd_2O_3 . No signal of other phases can be detected. SEM and TEM observations (Fig. 5) revealed that the rod-like shape is maintained after calcination, but the surface of these nanorods becomes rough. Further HRTEM observation indicates that the surfaces of the nanorods are

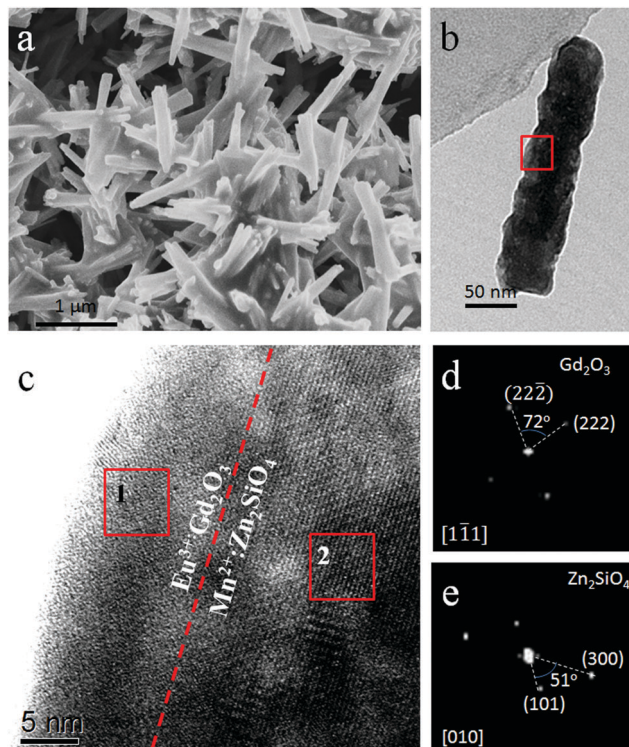


Fig. 5 (a) SEM and (b) TEM images of the $\text{Mn}^{2+}:\text{Zn}_2\text{SiO}_4\text{-Eu}^{3+}:\text{Gd}_2\text{O}_3$ composite product, (c) HRTEM of an individual $\text{Mn}^{2+}:\text{Zn}_2\text{SiO}_4\text{-Eu}^{3+}:\text{Gd}_2\text{O}_3$ nanocomposite, (d) and (e) FFT patterns taken from region 1 and region 2 labeled by red frames, respectively.

densely covered by many ~ 5 nm sized nanoparticles (Fig. 5c). According to FFT patterns taken from surficial and body regions, respectively, it is concluded that the rod-body is hexagonal Zn_2SiO_4 , while the surficial nanoparticles are cubic Gd_2O_3 , as shown in Fig. 5d and e.

3.2. Luminescence properties of the products

Fig. 6 presents the photoluminescence (PL) and photoluminescence excitation (PLE) spectra of the $\text{Mn}^{2+}:\text{Zn}_2\text{SiO}_4$ nanorods

and $\text{Mn}^{2+}:\text{Zn}_2\text{SiO}_4\text{-Eu}^{3+}:\text{Gd}_2\text{O}_3$ nanocomposites. As shown in Fig. 6a, for the $\text{Mn}^{2+}:\text{Zn}_2\text{SiO}_4$ nanorods, a bright green emission that peaked at 520 nm is observed, which is ascribed to the ${}^4\text{T}_1 \rightarrow {}^6\text{A}_1$ transition of the Mn^{2+} ions. In the PLE spectrum, the band detected at 260 nm is attributed to the Mn–O charge transfer (CT) state.²⁸ For the $\text{Mn}^{2+}:\text{Zn}_2\text{SiO}_4\text{-Eu}^{3+}:\text{Gd}_2\text{O}_3$ nanocomposites, except for emission from the Mn^{2+} ions, typical Eu^{3+} emissions (peaked at 580 nm, 612 nm and 625 nm) ascribed to the ${}^5\text{D}_0 \rightarrow {}^7\text{F}_1, {}^7\text{F}_2$ transition can also be observed (Fig. 6b). It is noted in the PLE spectra that the band ascribed to Eu–O CT also located at 260 nm is just similar to that of Mn–O CT. In other words, 260 nm light can excite the emissions of both Eu^{3+} and Mn^{2+} ions.

As presented by the temperature-dependent PL spectra shown in Fig. 7a, with an increase of temperature from 303 K to 623 K, the Mn^{2+} emission weakens rapidly, while the Eu^{3+} emission exhibits only a relatively slight decrease. The remarkable change in the FIR (*i.e.* $I_{\text{Eu}}/I_{\text{Mn}}$, see Fig. 7b) induces the shift of emission color from green to red, as indexed in the inset of Fig. 7a and the Commission International ed'Eclairage (CIE) diagram presented in Fig. 7c. These results imply the $\text{Mn}^{2+}:\text{Zn}_2\text{SiO}_4\text{-Eu}^{3+}:\text{Gd}_2\text{O}_3$ nanocomposite to be a promising candidate for luminescence thermometric application. And the small size and uniform shape of this material also benefit the spatial resolution in temperature sensing.

3.3. Origination of the temperature-dependent luminescence

To explain the origination of such diverse temperature dependence for Mn^{2+} and Eu^{3+} luminescence, the schematic configurational coordinate diagrams for a “strong coupling” system (Mn^{2+}) and a “weak coupling” system (Eu^{3+}) are presented in Fig. 8. Obviously, the thermal quenching dynamics for these two systems are totally different. For the “strong coupling” system, a parabola for the excitation state is not parallel to that for the ground state in the configurational coordinate,²⁵ as shown in Fig. 8a. Thermal quenching occurs when the electrons populated at the bottom of the excitation state migrate to the intersection between parabolas of the excitation and ground

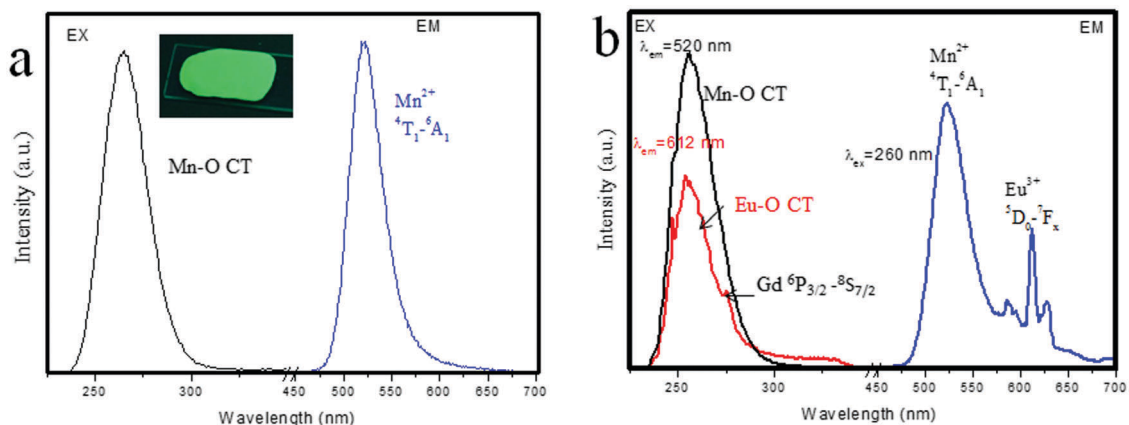


Fig. 6 (a) Photoluminescence (PL) and photoluminescence excitation (PLE) spectra of the $\text{Mn}^{2+}:\text{Zn}_2\text{SiO}_4$ nanorods; the inset in (a) shows the photograph of the $\text{Mn}^{2+}:\text{Zn}_2\text{SiO}_4$ nanorods under ultraviolet (255 nm) excitation. (b) PL and PLE spectra of $\text{Mn}^{2+}:\text{Zn}_2\text{SiO}_4\text{-Eu}^{3+}:\text{Gd}_2\text{O}_3$ nanocomposites.

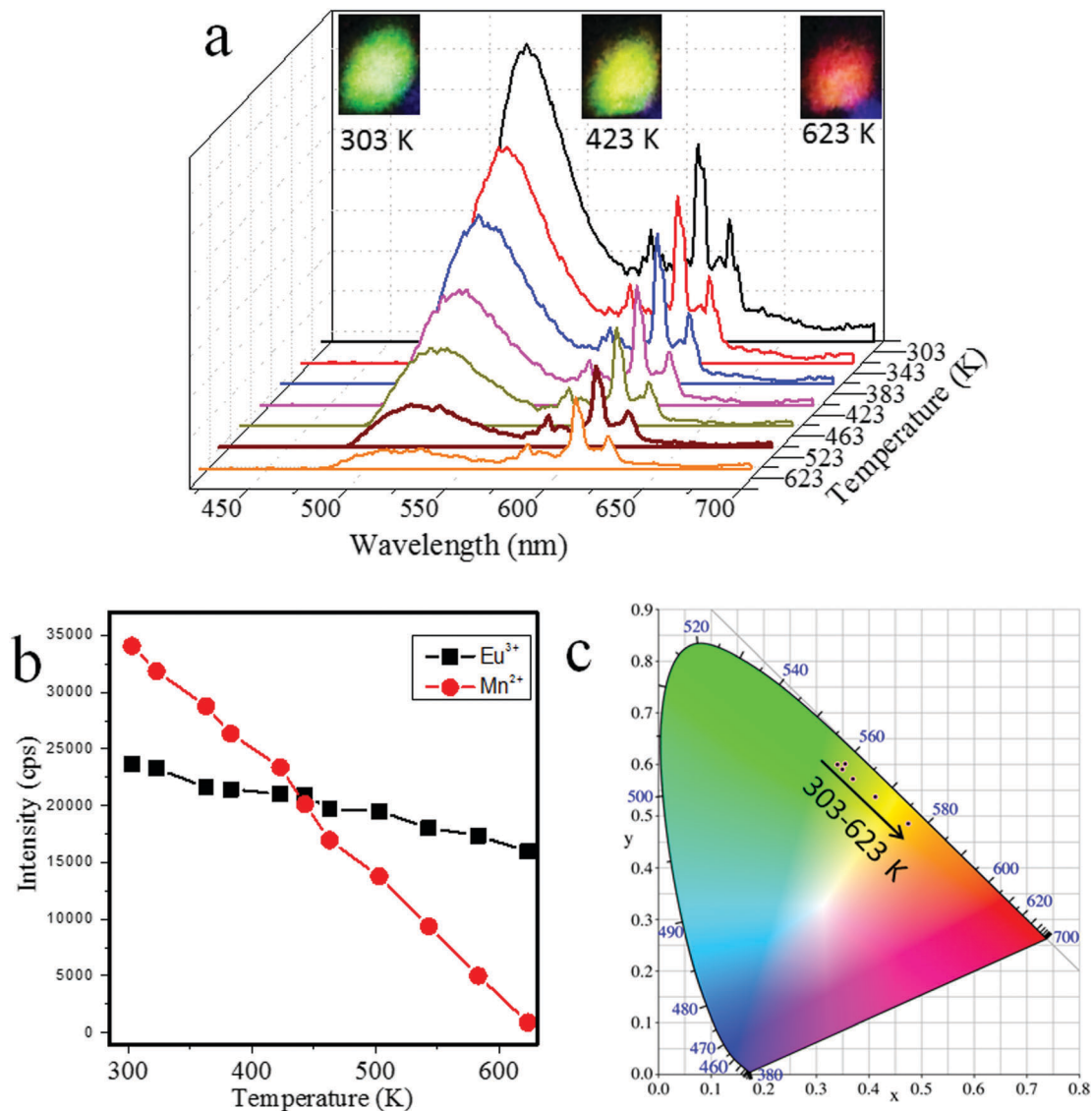


Fig. 7 (a) Temperature-dependent PL spectra of the $\text{Mn}^{2+}:\text{Zn}_2\text{SiO}_4-\text{Eu}^{3+}:\text{Gd}_2\text{O}_3$ nanocomposites under 260 nm excitation; insets show the photos of the sample under UV excitation, taken at 303, 423 and 623 K respectively. (b) Plots of intensity versus temperature for both Mn^{2+} and Eu^{3+} luminescence. (c) CIE (x, y) coordinate diagram of the emission color at various temperatures.

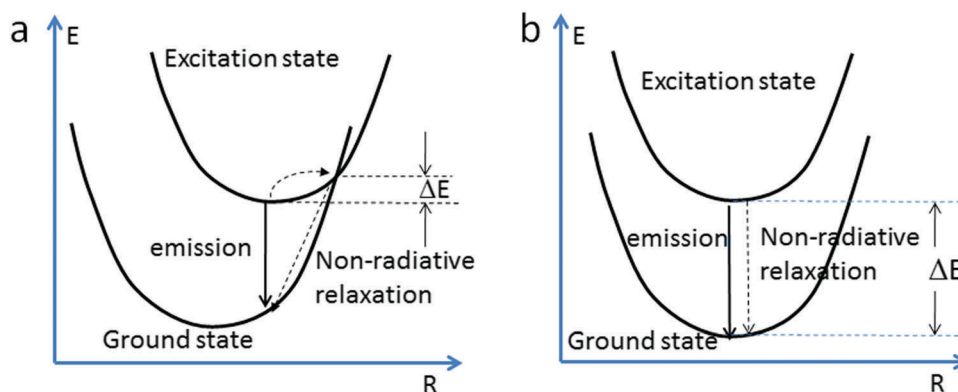


Fig. 8 Schematic configurational coordinate diagrams for a (a) "strong coupling" system and (b) "weak coupling" system.

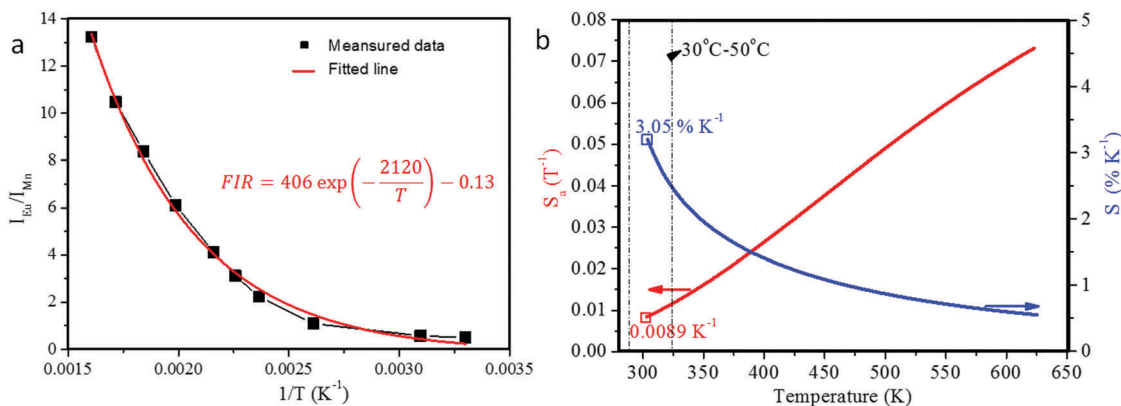


Fig. 9 (a) Experimentally measured and eqn (3) fitted plots of FIR ($I_{\text{Eu}}/I_{\text{Mn}}$) versus temperature. (b) Absolute sensitivity S_a and relative sensitivity S_r versus temperature.

states, and then relax there. The relationship between temperature (T) and PL intensity (I) can be expressed as:

$$\frac{I(T)}{I_0} = \frac{1}{1 + A \exp(-\Delta E/kT)} \quad (1)$$

where I_0 is the PL intensity at 0 K, A is a pre-exponential constant, k is the Boltzmann constant, T is the absolute temperature, and ΔE is the quenching activate energy representing the distance from the bottom of the excitation state to the intersection between the excitation and ground states.

While for the “weak coupling” system, parabolas for the excitation and ground states are nearly parallel, as shown in Fig. 8a. The thermal quenching process follows the phonon-participant transition from the excitation state to the ground state, which is a typical high order process, and therefore possesses low probability, especially when the energy gap (ΔE) between the excitation and ground states is much high than the phonon energy of the host.^{26,27} The relationship between temperature (T) and PL intensity (I) from this system can be expressed as:

$$\frac{I(T)}{I_0} = \frac{1}{1 + B \left[\frac{1}{1 - \exp(-\hbar\omega/kT)} \right]^P} \quad (2)$$

where I_0 is the PL intensity at 0 K, k is the Boltzmann constant, T is the absolute temperature, $\hbar\omega$ is the available phonon energy of the host, P is the number of phonons needed for relaxation from the excitation to the ground state (typically, $P = \Delta E/\hbar\omega$), and B is a parameter related to the radiative transition rate. For the Gd_2O_3 host, the highest phonon energy is about 600 cm^{-1} ,²⁹ much lower than the energy space between $^5\text{D}_0$ and $^7\text{F}_6$ (about $12\,200 \text{ cm}^{-1}$).³⁰ This explains the relative obtuseness of Eu^{3+} luminescence against increasing temperature, in $\text{Mn}^{2+}:\text{Zn}_2\text{SiO}_4-\text{Eu}^{3+}:\text{Gd}_2\text{O}_3$ nanocomposites.

3.3. Temperature sensitivities of the $\text{Mn}^{2+}:\text{Zn}_2\text{SiO}_4-\text{Eu}^{3+}:\text{Gd}_2\text{O}_3$ nanocomposites

To further evaluate the temperature sensing performance of $\text{Mn}^{2+}:\text{Zn}_2\text{SiO}_4-\text{Eu}^{3+}:\text{Gd}_2\text{O}_3$ nanocomposites, the theoretical relationship between temperature and the FIR of Mn^{2+} to

Eu^{3+} is deduced from eqn (1) and (2). With reasonable approximation, the equation of FIR versus T can be written as:

$$\begin{aligned} \text{FIR} &= \frac{I_{\text{Eu}}}{I_{\text{Mn}}} = \frac{I_{0,\text{Eu}}}{I_{0,\text{Mn}}} \frac{1 + A \exp(-\Delta E/kT)}{1 + B[1 - \exp(-\hbar\omega/kT)]^{-P}} \\ &\approx C + D \exp(-E/kT) \end{aligned} \quad (3)$$

where C , D and E are the parameters related to the constants of Mn^{2+} and Eu^{3+} ions in $\text{Mn}^{2+}:\text{Zn}_2\text{SiO}_4-\text{Eu}^{3+}:\text{Gd}_2\text{O}_3$ nanocomposites. A detailed deducing process is presented in the ESI.† The absolute and relative temperature sensitivities, S_a and S_r , can be further derived and expressed using the following equations:

$$S_a = \left| \frac{\partial \text{FIR}}{\partial T} \right| = D \exp(-E/kT) \times \frac{E}{kT^2} \quad (4)$$

$$S_r = 100\% \times \left| \frac{1}{\text{FIR}} \frac{\partial \text{FIR}}{\partial T} \right| = 100\% \times \frac{D \exp(-E/kT)}{C + D \exp(-E/kT)} \times \frac{E}{kT^2} \quad (5)$$

As displayed in Fig. 9a, the measured plots of FIR versus temperature can be fitted well by eqn (3). Herein, parameter C is fitted to be a minus, which may be owing to the approximation made in deducing eqn (3). The S_a and S_r values then calculated using eqn (4) and (5) are presented in Fig. 9b. Noteworthy, in the room temperature range (303–323 K, *i.e.* 30–50 °C), $\text{Mn}^{2+}:\text{Zn}_2\text{SiO}_4-\text{Eu}^{3+}:\text{Gd}_2\text{O}_3$ nanocomposites exhibit remarkably high temperature sensitivities. The values of S_r in this temperature range are all beyond $2.5\% \text{ K}^{-1}$, and reach as high as $3.05\% \text{ K}^{-1}$ at 303 K; while the values of S_a in this temperature range are all beyond 0.0089 K^{-1} . This performance is superior to most of the inorganic optical thermometric materials reported before.

4. Conclusions

In this study, a composite for nano-thermometry ($\text{Mn}^{2+}:\text{Zn}_2\text{SiO}_4$ nanorod coated with $\text{Eu}^{3+}:\text{Gd}_2\text{O}_3$ nanoparticles) is constructed following a multi-step solution route. This optical thermometric nanomaterial integrates “strong coupling” activators

(*i.e.* Mn²⁺ ions) and “weak coupling” ones (*i.e.* Eu³⁺ ions) within a single nanostructure, therefore exhibits a FIR with remarkable temperature sensitivity. In particular, in the room temperature range, S_a and S_r of this nano-thermometry are extremely high ($S_a = 3.05\% \text{ K}^{-1}$ and $S_r = 0.0089 \text{ K}^{-1}$ at 303 K), being superior to most of the other inorganic thermometric materials reported before. Possessing small grain size and high sensitivity at room temperature, this material can be regarded as a very promising nano temperature probe.

Acknowledgements

This work was supported by the National Natural Science Foundation of China (Grant No. 11574312).

References

- C. D. S. Brites, P. P. Lima, N. J. O. Silva, A. Millán, V. S. Amaral, F. Palacio and L. D. Carlos, *Adv. Mater.*, 2010, **22**, 4499–4504.
- L. H. Fischer, G. S. Harms and O. S. Wolfbeis, *Angew. Chem., Int. Ed.*, 2011, **50**, 4546–4551.
- B. Dong, B. S. Cao, Y. Y. He, Z. Liu, Z. P. Li and Z. Q. Feng, *Adv. Mater.*, 2012, **24**, 1987–1993.
- X. T. Rao, T. Song, J. K. Gao, Y. J. Cui, Y. Yang, C. D. Wu, B. L. Chen and G. D. Qian, *J. Am. Chem. Soc.*, 2013, **135**, 15559–15564.
- X. D. Wang, O. S. Wolfbeis and R. J. Meier, *Chem. Soc. Rev.*, 2013, **42**, 7834–7869.
- S. H. Zheng, W. B. Chen, D. Z. Tan, J. J. Zhou, Q. B. Guo, W. Jiang, C. Xu, X. F. Liu and J. R. Qiu, *Nanoscale*, 2014, **6**, 5675–5679.
- D. Q. Chen, Z. Y. Wan, Y. Zhou, X. Z. Zhou, Y. L. Yu, J. S. Zhong, M. Y. Ding and Z. G. Ji, *ACS Appl. Mater. Interfaces*, 2015, **7**, 19484–19493.
- J. Lee, H. Yang, C. H. Park, H. H. Cho, H. Yun and B. J. Kim, *Chem. Mater.*, 2016, **28**, 3446–3453.
- W. Xu, H. Zhao, Y. X. Li, L. J. Zheng, Z. G. Zhang and W. W. Cao, *Sens. Actuators, B*, 2013, **188**, 1096–1100.
- A. Benayas, B. del Rosal, A. Perez-Delgado, K. Santacruz-Gomez, D. Jaque, G. Alonso Hirata and F. Vetrone, *Adv. Opt. Mater.*, 2015, **3**, 687–694.
- F. Huang, Y. Gao, J. C. Zhou, J. Xu and Y. S. Wang, *J. Alloys Compd.*, 2015, **639**, 325–329.
- D. Q. Chen, Z. Y. Wan and S. Liu, *Anal. Chem.*, 2016, **88**, 4099–4106.
- D. Jaque and F. Vetrone, *Nanoscale*, 2012, **4**, 4301–4326.
- C. D. S. Brites, P. P. Lima, N. J. O. Silva, A. Millán, V. S. Amaral, F. Palacio and L. D. Carlos, *Nanoscale*, 2012, **4**, 4799–4829.
- M. H. Liu, M. Gu, Y. Tian, P. Huang, L. Wang, Q. F. Shi and C. E. Cui, *J. Mater. Chem. C*, 2017, **5**, 4025–4033.
- Y. Y. Tian, Y. Tian, P. Huang, L. Wang, Q. F. Shi and C. E. Cui, *Chem. Eng. J.*, 2016, **297**, 26–34.
- Y. Tian, B. N. Tian, C. E. Cui, P. Huang, L. Wang and B. J. Chen, *RSC Adv.*, 2015, **5**, 14123–14128.
- W. Xu, Z. G. Zhang and W. W. Cao, *Opt. Lett.*, 2012, **37**, 4865–4867.
- X. S. Lian, D. Zhao, Y. J. Cui, Y. Yang and G. D. Qian, *Chem. Commun.*, 2015, **51**, 17676–17679.
- S. S. Zhou, X. T. Wei, X. Y. Li, Y. H. Chen, C. K. Duan and M. Yin, *Sens. Actuators, B*, 2017, **246**, 352–357.
- W. Tang, S. C. Wang, Z. L. Li, Y. Sun, L. M. Zheng, R. Zhang, B. Yang, W. W. Cao and M. Yu, *Appl. Phys. Lett.*, 2016, **108**, 061902.
- Y. Gao, F. Huang, H. Lin, J. C. Zhou, J. Xu and Y. S. Wang, A novel optical thermometry strategy based on diverse thermal response from two intervalence charge transfer states, *Adv. Funct. Mater.*, 2016, **26**, 3139–3145.
- Y. Gao, F. Huang, H. Lin, J. Xu and Y. S. Wang, *Sens. Actuators, B*, 2017, **243**, 137–143.
- M. K. Kreto, I. M. Iskandarova, B. V. Potapkin, A. V. Scherbinin, A. M. Srivastava and N. F. Stepanov, *J. Lumin.*, 2012, **132**, 2143–2150.
- G. Blasse, *Prog. Solid State Chem.*, 1988, **18**, 79.
- S. Shionoya and W. M. Yen, *Phosphor Handbook*, CRC Press, 1998, p. 423.
- G. Blasse and B. Grabmaier, *Luminescent Materials*, Springer-Verlag, Berlin, 1994.
- J. S. An, J. H. Noh, I. S. Cho, H. S. Roh, J. Y. Kim, H. S. Han and K. S. Hong, *J. Phys. Chem. C*, 2010, **114**, 10330–10335.
- H. Guo, N. Dong, M. Yin, W. P. Zhang, L. R. Lou and S. D. Xia, *J. Phys. Chem. B*, 2004, **108**, 19205–19209.
- P. A. Tanner, Y. Y. Yeung and L. X. Ning, *J. Phys. Chem. A*, 2013, **117**, 2771–2781.